Distribution of magnetization of a cold ferromagnetic cluster beam

Xiaoshan Xu, Shuangye Yin, Ramiro Moro, and Walt A. de Heer
School of Physics, Georgia Institute of Technology, Atlanta, Georgia 30332, USA
(Received 29 May 2008; published 20 August 2008)

Above a critical temperature, a supported single domain ferromagnetic particle responds to an applied magnetic field as if it were a paramagnet with a very large spin. Its average magnetization is given by the Langevin equation as expected from simple thermodynamic considerations. The average magnetization of an ensemble of unsupported ferromagnetic clusters also approximately follows the Langevin equation even for small clusters in a low-temperature ensemble. The reason is not obvious because there is no heat bath for low-energy clusters so that elementary thermodynamic requirements for the Langevin equation are not satisfied. We investigated the magnetic deflections of cobalt clusters (Co_N, $12 \le N \le 200$) using molecular-beam methods over a wide range of temperatures ($20 \le T \le 100$ K) and magnetic fields ($0 \le B \le 2$ T). A distribution of magnetization is observed for the cluster beams. Previously, we showed that the average magnetization of the cluster beam follows Langevin function closely for all temperatures and magnetic fields investigated, and proposed an avoided-crossing model that takes into account interacting spin-rotational states. In this paper, we report a comprehensive study of the magnetization distribution and present in depth the avoided-crossing model. The model explains both the average and the width of the magnetization distributions of the cluster beam in terms of the ensemble temperature without requiring that individual clusters have defined temperatures. We also show that the spin-relaxation model is the high-temperature limit of the avoided-crossing model.

DOI: 10.1103/PhysRevB.78.054430 PACS number(s): 75.20.−g, 36.40.Cg, 73.22.−f

I. INTRODUCTION

Molecular-beam method is a compelling way to measure the intrinsic magnetic properties of individual isolated ferromagnetic clusters.[1–19] In molecular-beam experiments, the magnetic properties of the small particles are studied by measuring the deflections of a beam in an inhomogeneous magnetic field (Stern-Gerlach magnet). The deflection of a single small particle with magnetic moment μ is proportional to its magnetization $M_{\text{single}} \equiv \langle \mu_z \rangle_{\text{TAM}}$, where μ_z is the projection of its magnetic dipole moment along the applied magnetic field and $\langle\ \rangle_{\text{TAM}}$ denotes time average over the measurement. However, real experiments cannot distinguish every single particle, therefore what is measured is the distribution of the single-particle magnetization $P(M_{\text{single}})$. To characterize the distribution, we define

$$M = \frac{\int M_{\text{single}} P(M_{\text{single}}) dM_{\text{single}}}{\int P(M_{\text{single}}) dM_{\text{single}}},$$

$$\Delta M = \sqrt{\frac{\int (M_{\text{single}} - M)^2 P(M_{\text{single}}) dM_{\text{single}}}{\int P(M_{\text{single}}) dM_{\text{single}}}},$$

which come from the first and the second moments of the distribution, respectively. Note that M is actually the average magnetization of the beam and ΔM is the width of the distribution.

If such an experiment is performed on a beam of atoms with magnetic moment μ, the average magnetization of the beam M will be zero, as in the well-known Stern-Gerlach experiment. That is because μ_z of a certain atom does not change during the time of measurement and the probability to have every possible μ_z is the same. That is $-\mu \le M^{\text{single}} \le \mu$ and $P(M_{\text{single}}) = \text{const}$ (see Table I). Therefore, $M = 0$. On the other hand, it is well known that the magnetization of an atom deposited on a substrate is $M^{\text{single}}/\mu = \langle \mu_z \rangle_{\text{TAM}}/\mu = B_r(\mu B/k_B T)$, where B_r is the Brillouin function, B is the magnetic field, and T is the temperature of the substrate. The ensemble average gives the same results as for single atom: $M = M^{\text{single}}$. In the limit of large μ,the Brillouin function reduces to Langevin function, giving

$$M/\mu = L(\mu B/k_B T), \tag{1}$$

where $L(x) = \coth(x) - 1/x$ is the Langevin function. This follows from the thermodynamics of free magnetic moment μ in a magnetic field. However, it requires the atom to be in contact with a heat bath with a well defined temperature T.

In the low-field limit $\mu B/k_B T \to 0$,

$$M/\mu = L(\mu B/k_B T \to 0) = \mu B/3k_B T. \tag{2}$$

In the high-field limit,

$$M/\mu = 1. \tag{3}$$

The Langevin function also applies to supported ferromagnetic clusters (i.e., small single domain ferromagnetic particles), for temperatures above the blocking temperature. (That is when the thermal energy is larger than its magnetic anisotropy energy. Below this temperature, the spin is locked along an anisotropy axis, which reduces the response.) Because the Langevin function not only applies for paramagnetic atoms, but also for particles with very large spins, the latter are called superparamagnetic.[20] This nomenclature leads to much confusion since in fact superparamagnetic particles are actually ferromagnetic.

TABLE I. Comparison of the distribution of magnetization of atoms and magnetization of clusters in a beam and on a substrate.

	Atoms	Clusters
In a beam	$-\mu \leq M_{\text{single}} \leq \mu$	$0 < M_{\text{single}} \leq \mu$
	$P(M_{\text{single}})$=const	$P(M_{\text{single}})$: broad and asymmetric
	$M=0$	$M/\mu = B_r(\mu B/k_B T)$
	$\Delta M = \mu/\sqrt{3}$	$\Delta M > 0$
On a substrate (above the blocking temperature)	$M_{\text{single}} = B_r(\mu B/k_B T)$	$M_{\text{single}} = B_r(\mu B/k_B T)$
	$P(M_{\text{single}}) = \delta[M_{\text{single}} - \mu B_r(\mu B/k_B T)]$	$P(M_{\text{single}}) = \delta[M_{\text{single}} - \mu B_r(\mu B/k_B T)]$
	$M/\mu = B_r(\mu B/k_B T)$	$M/\mu = B_r(\mu B/k_B T)$
	$\Delta M = 0$	$\Delta M = 0$

Magnetic deflections of ferromagnetic clusters in a beam might be expected to be similar to those of atoms with a very large spin S and magnetic moment μ in which case the magnetization distribution is flat within the range $-\mu \leq M^{\text{single}} \leq \mu$ and consequently $M=0$. However, the magnetization of ferromagnetic cluster beams resembles that of supported ferromagnetic particles: M of the beam is polarized in the direction of the applied magnetic field. Moreover, experimentally for $\mu B/k_B T \ll 1$, $M \approx \mu^2 B/3k_B T$,[3,21] similarly for supported atoms and supported ferromagnetic clusters above the blocking temperature. (Here T is the ensemble temperature of the cluster beam.) Therefore, the behavior of the ferromagnetic clusters in a beam is also called superparamagnetism.

These observations of superparamagnetism in cluster beams led Khanna and Linderoth, in their spin-relaxation model (SRM), to assume that the thermodynamics of free clusters is equivalent to that of a supported cluster. This in turn requires that a free cluster, even with very few atoms and with low energy, must not only have a well defined temperature but the spin must equilibrate with that temperature when the cluster is in the magnetic field. While this point of view may be justified for large isolated clusters at relatively high energy, it is not clear how it applies to small isolated clusters with low energy. Nevertheless, the SRM has been used as the origin of Langevin function [Eq. (1)] universally to extract cluster magnetic moments form molecular-beam deflection data, which have been extensively compared with theory.[18,21–31] However, no matter how successful SRM is, one has to keep in mind that SRM is only part of the story because it ignores the fact that the distribution $P(M_{\text{single}})$ is in general different for clusters in a beam and for clusters on a substrate, as summarized in Table I. To have the complete picture of superparamagnetism for clusters in a beam, the distribution $P(M_{\text{single}})$ needs to be understood better. The distribution $P(M_{\text{single}})$ has seldom been studied systematically, especially its temperature and field dependences. Previously, we have reported studies of magnetic moment (μ) and average magnetization (M) of cobalt clusters in cold beams.[19] We also proposed the avoided-crossing model to explain the average magnetization. In this paper, we performed comprehensive study of the distribution $P(M_{\text{single}})$ of cobalt cluster beams over a large range of cluster sizes, magnetic fields, and temperatures. We also present in more detail the avoided-crossing model that explains both the average and the width of the distribution $P(M_{\text{single}})$ of the cluster beams quantitatively. We will show that the SRM can be understood as the high-temperature limit of the avoided-crossing model.

II. EXPERIMENT

The magnetic deflection experiment is briefly described next (see also Refs. 15, 17, and 18). A beam of cobalt cluster is generated in a cryogenically cooled laser ablation source, the temperature of which can be varied from $T=15-300$ K. The clusters thermalize in the ≈ 0.5 cm^3 source chamber so that the cluster ensemble has the same temperature as the source. After that, the clusters exit the nozzle (1 mm diameter) and enter the collision-free drift chamber. The cluster beam is collimated by two 0.3-mm-wide slits. The clusters are deflected in the inhomogeneous field of Stern-Gerlach magnet ($B \leq 2$ T and $dB/dz = 0.25B$ T/cm) 1 m downstream from the source. The clusters are then photoionized with light from an ArF excimer laser 2 m downstream from the source and enter a position-sensitive time-of-flight (PSTOF) mass spectrometer. The PSTOF simultaneously records the positions and the masses of the ionized clusters. The data are electronically recorded for further analysis. The clusters' speeds and their dwell times in the source are accurately determined using a mechanical chopper 10 cm downstream from the nozzle.

The average magnetization M_N of a beam of clusters with N atoms with mass m_N and velocity v in a magnetic field B with field gradient dB/dz is determined from its deflection d_N using

$$M_N(B) = K m_N v^2 d_N/(dB/dz), \tag{4}$$

where K is a geometrical constant of the experimental apparatus.

A. Distribution of magnetization of the cluster beam

We reiterate the results reported in Ref. 18. Figure 1(a) shows an example of beam profiles for Co_{20} at $T=40$ K and $B=2$ T. Note two important features: (i) the clusters deflect exclusively in the direction of increasing field strength; (ii) the beam profile is significantly broadened when the field is

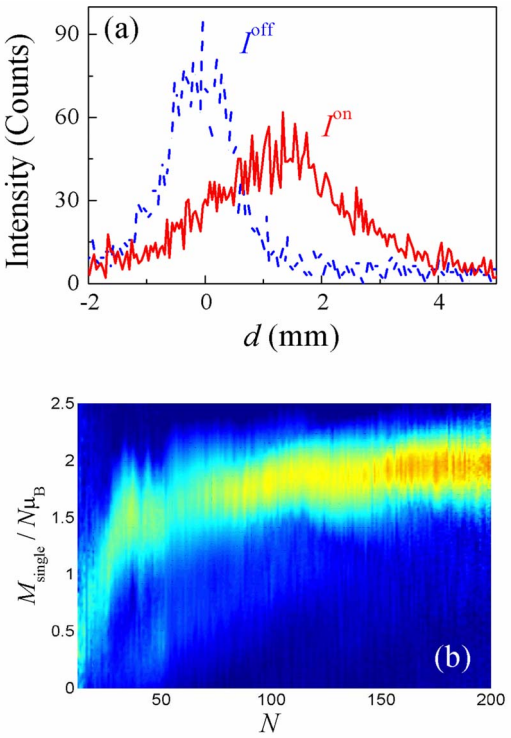

FIG. 1. (Color online) Deflections and magnetization distributions of Co_N at $T=40$ K and $B=2$ T. (a) Position sensitive PSTOF mass peak of Co_{20} showing the field off (dashes) and the field on ($B=2$ T, solid) deflections (the entire spectrum is composed of about 200 distinct mass peaks). Note the single-sided deflections. (b) Normalized magnetization distributions $P(M_{single})$ of $Co_N(12 \leq N \leq 200$, $T=40$ K, $B=2$ T). Brighter (red) color means high value of $P(M_{single})$; darker (blue) color means low. The average magnetization is linear with N for small N and saturates at about $\mu_N \approx 2N\mu_B$ for large N.

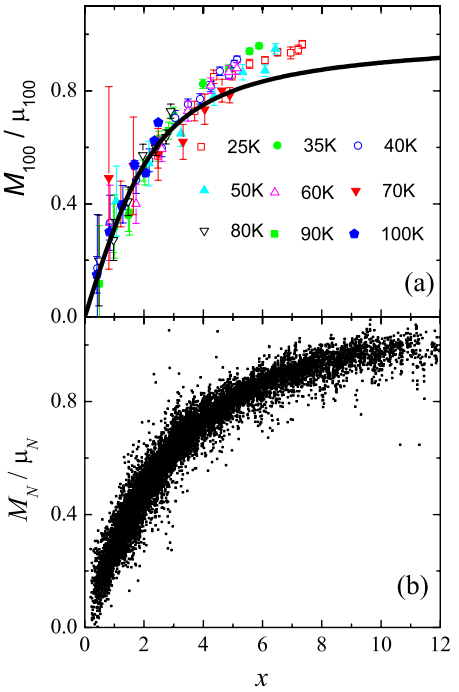

FIG. 2. (Color online) Normalized magnetizations M_N/μ_N of Co_N. (a) M_N/μ_N of Co_{100} for 25 K $\leq T \leq$ 100 K and $0 \leq B \leq 2$ T, corresponding to x ranging from 0.4 to 12. The data scale with x. Note the linear increase for small x: $M_{100}/\mu_{100} \approx 0.3x$ and $M_{100}/\mu_{100}=1$ for large x. The trend is consistent with the Langevin function (bold line); however, the Langevin function approaches saturation more slowly. (b) M_N/μ_N for $12 \leq N \leq 200$, 20 K $\leq T \leq$ 100 K, and $B \leq 2$ T measured in 63 data sets (nine temperatures from 25 to 100 K and seven fields from 0 to 2 T, representing about 10 000 data points), plotted as a function of x.

on. The magnetization distribution $P(M_{single})$ is extracted from the beam profiles with magnetic field off $I^{off}(d)$ and magnetic field on $I^{on}(d)$ using a deconvolution procedure that takes into account the width of the collimated beam. In Fig. 1(b) the magnetization distributions $P(M_{single})$ of all of the clusters are plotted where the color represents the value. Note that the magnetization per atom with maximum intensity saturates at about $2\mu_B$ for large clusters.

B. Average of magnetization distribution

A detailed analysis of the magnetization data follows. Quite generally when $\mu B/k_BT \gg 1$ the magnetization saturates at the magnetic moment value: $M=\mu$ (for a cluster with N atoms, $M=\mu_N$). This allows a direct determination of the magnetic moment. Next consider the experimental relation for cluster with N atoms $M_N/\mu_N=f(x)$, where $x=\mu_N B/k_BT$. For large clusters the relation $f(x)$ found from different fields, temperatures and sizes falls on a universal curve [Fig. 2(a)], which resembles the Langevin function $L(x)$, as indicated by the bold line. In the low x range $f(x)$ matches $L(x)$ very well. Note, however, that for large x, $f(x)$ saturates faster than predicted by $L(x)$. For smaller clusters (which have proportionally smaller magnetic moments), the available magnetic fields (2 T) are too small to saturate the magnetization. We extrapolate the magnetic moments of small clusters by scaling their magnetization curves to the universal curve. Since T and B are known, μ is determined. Figure 2(b) shows the magnetization curve $M_N/\mu_N=f(x)$ for all cluster sizes investigated. The universal curve $f(x)$ is represented by more than 10 000 experimental points. The magnetic moments per atom for all cluster sizes found in this way, are consistent with previously determined values.[3,4,8] This is not too surprising since previously the low-field equation [Eq. (2)] was used, which also represents the low-field limit of the universal curve. Note that the magnetic moments oscillate with the cluster size with maxima near $N=37$; and minima at $N=23$, 41, 51, 83, and 121.[18] The magnetic moments converge to about $2\mu_B$ per atom for $N>150$.

C. Width of magnetization distribution

As shown in Fig. 1(b), the magnetization distribution of a cluster beam has a significant width. To analyze this width, we investigate the broadening of the beam profiles when the magnetic field is turned on. Suppose the beam profiled with field off and field on are $I^{off}(d)$ and $I^{on}(d)$, respectively, where d is the deflection. The beam broadening ΔW is defined as

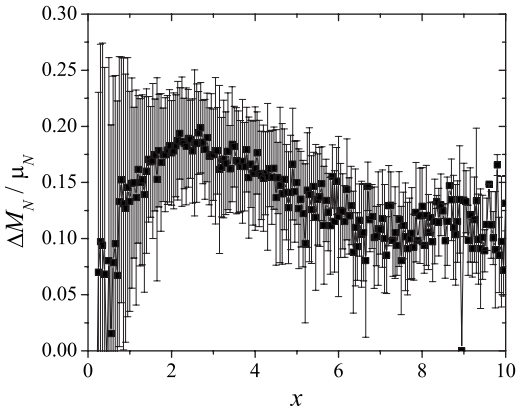

FIG. 3. The normalized width of magnetization distribution $\Delta M_N/\mu_N$ as a function of x. The data points are found by averaging the values of $\Delta M_N/\mu_N$ for cluster conditions over a small range of x. Note that the second moment of a beam profile is more sensitive to random noise than its first moment, which brings significant uncertainty.

$$\Delta W \equiv \sqrt{W_{\text{on}}^2 - W_{\text{off}}^2},$$

where W_{on}^2 is second moment of $I^{\text{on}}(d)$ and W_{off}^2 is the second moment of $I^{\text{off}}(d)$. Equation (4) relates ΔW to the magnetization distribution width ΔM if one treats ΔW as deflection (see Fig. 3). Note that ΔM is small at low fields, increases to a maximum at intermediate fields, and decreases again at high fields.

III. LIMITATION OF THE SRM

To understand the observed magnetization distribution, we start with spin-relaxation model and why it is incomplete. The SRM relates the measured average magnetization of a cluster beam to the magnetic moment of the individual clusters using the Langevin equation [Eq. (1)], whose usage for small clusters in a low-temperature beam must be justified. The Langevin equation is derived for a canonical ensemble. In that case the particles contact a heat bath with a well defined temperature, with which it can exchange both energy and angular momentum. This is clearly not the case for an isolated cluster with low energy, and in order to justify the Langevin equation, it requires that the internal degrees of freedom of the cluster constitute an effective heat bath at a well defined temperature (presumably that of the source) and as a source of angular momentum. If not, then spin relaxation cannot be justified. While large clusters in a high-temperature beam may serve as their own heat bath and source of angular momentum because enough rotational, vibrational, and electronic degrees of freedom are activated, it is not the case for small clusters in a low-temperature beam with vibration and electronic excitation quenched. Consider a Co_N cluster with $N=20$ in a $T=50$ K beam (note that experimentally, we can achieve more extreme condition: e.g., $N=12$ and $T=20$ K), the electronic state separation is of the order of $E_F/N \approx 100$ meV, where E_F is the Fermi energy so that the clusters are in their electronic ground states. For such a small particle, the $3N-6$ vibrational modes have energy that all close to the Debye energy $E_D=k_B T_D$, where $T_D=445$ K is the Debye temperature for bulk cobalt. Hence, on average such a particle contains less than one excited vibrational mode. Therefore, neither the vibrations nor the electronic excitation can serve as a heat bath. This leaves the rotations that represent only three modes. It is clearly incorrect to consider the rotations as a thermodynamic heat bath; actually, it is better to describe an individual cluster in this case using its energy rather than using temperature because an isolated low-energy cluster should have a well defined energy while the definition of temperature may be vague. Moreover, for an isolated cluster, angular momentum conservation must be taken into account.[18,26,27,29–31] The total angular momentum of a cluster is a sum of three parts: $\boldsymbol{J}=\boldsymbol{R}+\boldsymbol{L}+\boldsymbol{S}$, where $\boldsymbol{R}$, $\boldsymbol{L}$, and $\boldsymbol{S}$ correspond to the angular momentum from the rigid body rotation, electronic orbital motion, and electronic spin, respectively. For iron group clusters, $\boldsymbol{L}$ is quenched. Thus, $\boldsymbol{J}=\boldsymbol{R}+\boldsymbol{S}$. When the clusters negotiate with the magnetic field, conservation of J_z (projection of total angular momentum J along the magnetic field) should not be ignored. However, in SRM, its direction must change freely in order to relax the spin, which is again unjustifiable for isolated low-energy clusters.

The SRM violates statistical thermodynamics and the angular momentum conservation for small clusters in low-temperature beams because of the missing heat and angular momentum bath. Nevertheless, the experiment (see Fig. 2) shows that the Langevin function [Eq. (1)] is a reasonable approximation of the average magnetization of the cluster beam even for small clusters in low-temperature beams.[18] Clearly, the Langevin function [Eq. (1)] is approximately valid even when the SRM fails. As shown below, spin alignment, which causes the nonzero average magnetization, can in fact be mediated by the rotations even for very small clusters in a very low-temperature beam. However, in contrast to the SRM, spin relaxation does not necessarily occur. In fact, the spin alignment effect is caused by avoided crossings in the spin-rotation Zeeman diagram, at least for small clusters in a low-temperature beam. We further show that the ensemble average magnetization M quite generally follows the Langevin equation both in the low-field and high-field limits and further that the temperature T is the temperature of the cluster beams not of individual clusters.

IV. AVOIDED-CROSSING MODEL

It is important to emphasize that the idea of the avoided-crossing model is to bring back the details that are ignored by the SRM and discuss them carefully in order to complete our understanding of the distribution of the magnetization of ferromagnetic clusters. Although we argue the importance of the avoided-crossing model especially for small clusters in a low temperature beam, it is actually a more general model that is more widely applicable than the SRM. Specifically, the rotational, vibrational, and electronic excitations are all accounted for in the model. It is also shown that when there are enough vibrational and electronic degrees of freedom excited the avoided-crossing model predicts the same behavior of the magnetization as the SRM does, say, very narrow dis-

tribution. In fact, the system of an isolated cluster is more ergodic when lots of degrees of freedom are activated, which is the case for high-temperature beams. Therefore, the SRM that comes from simple thermal dynamics is the high-temperature limit of the avoided-crossing model.

In the magnetic deflection experiments, clusters start from zero field, then enter the field and deflect. Therefore, the objective here is more than solving the Hamiltonian and getting the stationary wave function. Instead, we shall be concerned with the Zeeman diagram where the evolution of eigenstates is defined. As shown below, we will find the eigenstates (as a function of the magnetic field) in the Zeeman diagram first, using the assumption of avoided-crossing. Then we populate these states according to the ensemble temperature and calculate the distribution of magnetization.

A. Hamiltonian of free ferromagnetic clusters

The general Hamiltonian for a cluster in the magnetic field is

$$H = H_E + H_V + H_R + H_{\text{couple}} - g\mu_B \mathbf{S} \cdot \mathbf{B}, \tag{5}$$

where H_E, H_V, H_R, and H_{couple} are, respectively, the parts for electronic excitation, vibration, rotation, and the coupling between the spin and rotational angular momentum, and g is the Lande factor (for clusters of iron group atoms, $g \approx 2$).

B. Physical process of Stern-Gerlach experiment

The physical process of the measurement the magnetization of a cluster in a Stern-Gerlach experiment is very different from that of a supported particle. Basically, clusters are generated and reach equilibrium in the source and form a canonical ensemble. However, every cluster interacts with the magnetic field independently because it is isolated.

1. Cluster generation

Clusters are generated in the source at temperature T in zero magnetic fields, where they populate states $\{\varphi_i^0,\ i=1,2\ldots\}$ with energy $\{E_i^{\text{EVR}},\ i=1,2\ldots\}$, respectively. We assume that H_{couple} is small compared to all the other terms in Eq. (5) (see Appendix A). Therefore, the zero-field eigenstates $\{\varphi_i^0,\ i=1,2\ldots\}$ are linear combinations of eigenstates of electronic excitations, vibrations, and rotations, and $\{E_i^{\text{EVR}},\ i=1,2\ldots\}$ are the linear combination of energy of those excitations (see Ref. 32 for the notation of various energies). The cluster population on state φ_i^0 is described by the Boltzmann distribution because clusters in the source can be considered as a canonical ensemble.

2. Adiabatic evolution of states

In the limit of vanishing coupling between the spin and rotations ($H_{\text{couple}}=0$), the energy of the ith state evolves as $E_i^{\text{uncouple}} = E_i^{\text{EVR}} - g\mu_B S_z^i B$ (dashed lines in Fig. 4). The magnetization of the uncoupled levels is simply $M_i^{\text{uncouple}} = -\partial E_i^{\text{uncouple}} / \partial B = g\mu_B S_z^i$.

However, the states are in general coupled and the angular momentum conservation should not be ignored. The real states that the clusters traverse are adiabatic (coupled) states explained below.

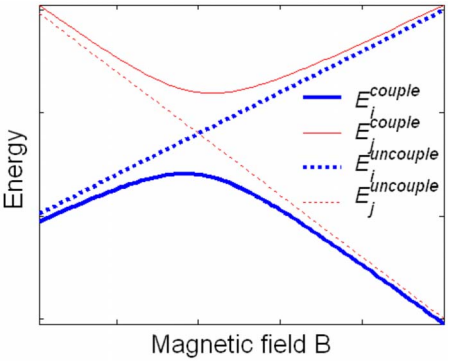

FIG. 4. (Color online) Schematic illustration of an avoided level crossing. Notice that the coupling makes the spin orientation "flip" at the degeneracy point since the crossing of the two levels is avoided.

Let us consider two states $\varphi_i^{\text{uncouple}}$ and $\varphi_j^{\text{uncouple}}$ with the same J_z but different E^{EVR} and S_z. Their energies are

$$E_i^{\text{uncouple}} = E_i^{\text{EVR}} - g\mu_B S_z^i B$$

and

$$E_j^{\text{uncouple}} = E_j^{\text{EVR}} - g\mu_B S_z^j B.$$

If $E_i^{\text{EVR}} > E_j^{\text{EVR}}$ and $S_z^i > S_z^j$ (or vice versa), at certain value of magnetic field $B=B_0$, the two levels cross, as shown in Fig. 4. In other words, accidental degeneracy occurs when

$$E_i^{\text{EVR}} - g\mu_B S_z^i B_0 = E_j^{\text{EVR}} - g\mu_B S_z^j B_0.$$

The spin-rotation coupling H_{couple} is very important at the vicinity of $B=B_0$ where the two levels interact causing avoided crossing in the Zeeman diagram (see Fig. 4). Here with the basis set $\{\varphi_i^{\text{uncouple}}, \varphi_j^{\text{uncouple}}\}$ the Hamiltonian can be written as the matrix,

$$H = \begin{bmatrix} E_i^{\text{uncouple}} & \Delta_{\text{SR}} \\ \Delta_{\text{SR}} & E_j^{\text{uncouple}} \end{bmatrix} = \begin{bmatrix} E_i^{\text{EVR}} - 2\mu_B S_z^i B & \Delta_{\text{SR}} \\ \Delta_{\text{SR}} & E_j^{\text{EVR}} - 2\mu_B S_z^j B \end{bmatrix},$$

where $\Delta_{\text{SR}} \equiv \langle \varphi_i^{\text{uncouple}} | H_{\text{couple}} | \varphi_j^{\text{uncouple}} \rangle$ is the matrix element that corresponds to the spin-rotation coupling. Near the crossings, the energies of the coupled states are

$$E_i^{\text{couple}} = \tfrac{1}{2}(E_i^{\text{EVR}} + E_j^{\text{EVR}} - g\mu_B S_z^i B - g\mu_B S_z^j B) + \tfrac{1}{2}\sqrt{(E_i^{\text{EVR}} + E_j^{\text{EVR}} - g\mu_B S_z^i B - g\mu_B S_z^j B)^2 + 4\Delta_{\text{SR}}^2},$$

$$E_j^{\text{couple}} = \tfrac{1}{2}(E_i^{\text{EVR}} + E_j^{\text{EVR}} - g\mu_B S_z^i B - g\mu_B S_z^j B) - \tfrac{1}{2}\sqrt{(E_i^{\text{EVR}} + E_j^{\text{EVR}} - g\mu_B S_z^i B - g\mu_B S_z^j B)^2 + 4\Delta_{\text{SR}}^2}.$$

These (coupled) levels are the true eigenstates of the clusters. If the change in magnetic field is slow enough, clusters should follow these levels precisely (see Appendix C), which is why they are also called adiabatic states.

The projections of the spin along magnetic field are not good quantum numbers for the coupled levels. We can only define the average spin projection as $\langle S_z\rangle_{i,\text{couple}} = -1/g\mu_B \partial E_i^{\text{couple}}/\partial B$. Several features should be pointed out here (see Fig. 4): (a) At the avoided crossing, the total magnetization of the two levels is conserved; $\langle S_z\rangle_{i,\text{couple}} + \langle S_z\rangle_{j,\text{couple}} = S_z^i + S_z^j$. (b) At the avoided crossing, $\langle S_z\rangle_{i,\text{couple}} = \langle S_z\rangle_{j,\text{couple}} = (S_z^i + S_z^j)/2$. (c) The $\langle S_z\rangle_{i,\text{couple}}$ of each of the two adiabatic states reverses its sign after the avoided crossing. It is not difficult to generalize (a) and (b) for multiple interacting levels;

$$\sum_i \langle S_z\rangle_{i,\text{couple}} = \sum_i S_z^i.$$

In the vicinity of the crossing, one has approximately

$$\langle S_z\rangle_{i,\text{couple}} = \frac{\sum_i S_z^i}{N_{\text{level}}}, \tag{6}$$

where N_{level} is the number of interacting levels.

In reality, the number of interacting states is much larger than two because the states E_i^{uncouple} are so dense even for certain J_z. For example, the rotational level spacing for cobalt clusters is of order $C_r \approx 4\times 10^{-5}/N^{5/3}$ eV. Hence, in the Zeeman diagram there will be about $1\times N^{5/3}$ avoided crossings per tesla.

To illustrate this process, Figs. 5(a) and 5(b) show the calculated adiabatic states for Co_{12} (assuming $S=12$), as well as the uncoupled levels on different scales. Figures 5(c) and 5(d) show examples of a few calculated adiabatic states in larger scales. It is important to notice again that in real experiment, the measurements are taken with magnetic-fields range $\Delta B \sim 10^{-3}-10^{-2}$ T, which corresponds to the scales of Figs. 5(a) and 5(b). This means fine details of the adiabatic states are not measured. Averaging the adiabatic states over ΔB produces average adiabatic states that are quite smooth. Figure 5(d) shows a global view of these averaged states revealing key features. At low fields, the states are parabolic. At high field the slopes saturate to a common value, which corresponds to the magnetic moment. Note that these curves in Figs. 5(c) and 5(d) represent eigenstates of the clusters, which are temperature independent. The topology of these Zeeman diagrams does not depend on temperatures but the populations of clusters on those adiabatic states do. In other words, temperature is not necessarily a property of a single cluster but is a property of the cluster ensemble.

All of the states monotonically decrease with increasing field, which at once explains why the deflections are single sided. At a given field, the cluster magnetization (i.e., its slope) is energy dependent. Since the energies are initially thermally distributed, this dispersion of the slopes is reflected in a broadening of the measured magnetization distribution. A quantitative description follows.

C. Magnetization of a single cluster

The magnetization of a specific cluster should be calculated for the adiabatic states because the clusters are supposed to follow these levels. The (smoothed) magnetization of an adiabatic state is the average over all the interacting uncoupled levels in a small field and energy range, as shown in Eq. (6), and illustrated in Fig. 5(a). Hence, the magnetization of a single cluster with energy E at magnetic field B is

$$M_{\text{single}}(E,B) = g\mu_B \frac{\sum_{-S}^{S} S_z D(E,S_z)}{\sum_{-S}^{S} D(E,S_z)},$$

where $D(E,S_z)$ is the number of uncoupled levels with E and S_z in the measurement range (a range ΔB centered at B). Note that $D(E,S_z)$ is actually the same as the number of states with S_z and zero-field energy E^{EVR}, where $E^{\text{EVR}} = E + g\mu_B S_z B$. This simple relation comes from the fact that E is the energy of the uncoupled states. Therefore, the sum over S_z should be transformed into the sum over the zero-field energy E^{EVR}. Since the number of states is usually large (see Sec. IV B 2), the sum can be approximated by an integral,

$$M_{\text{single}}(E,B) = g\mu_B \frac{\int S_z \rho(E^{\text{EVR}})dE^{\text{EVR}}}{\int \rho(E^{\text{EVR}})dE^{\text{EVR}}}$$

$$= \frac{\int (E^{\text{EVR}} - E)\rho(E^{\text{EVR}})dE^{\text{EVR}}}{\int \rho(E^{\text{EVR}})dE^{\text{EVR}}}. \tag{7}$$

where $\rho(E^{\text{EVR}})$ is the density of states of energy E^{EVR} at zero field. Equation (7) allows us to find the average slope of an adiabatic state over the measurement range, which is the same as the magnetization of a single cluster, without diagonalizing the Hamiltonian.

The topology of the Zeeman diagrams shown in Fig. 5 is not symmetric with energy simply because there is a lower boundary $E=-g\mu_B SB$ but not an upper one. In fact, when the magnetization of a single cluster is calculated using Eq. (7), there are always more states coming from high-energy part of the Zeeman diagram than those from low-energy part. Because states from high-energy part of the Zeeman diagram contributes positive magnetization, the result of Eq. (7) always gives $M_{\text{single}} > 0$, which explains that in the experiment clusters deflects exclusively toward the direction with stronger field.

1. High-field limit

At high field, Zeeman term $-g\mu_B \mathbf{S}\cdot\mathbf{B}$ dominate the total energy of a cluster, resulting saturation of the magnetization of a single cluster, which is illustrated by Fig. 5(d), in which all the adiabatic states have magnetization of

$$M_{\text{single}} = g\mu_B S = \mu. \tag{8}$$

This explains the saturation of magnetization found in the experiments.

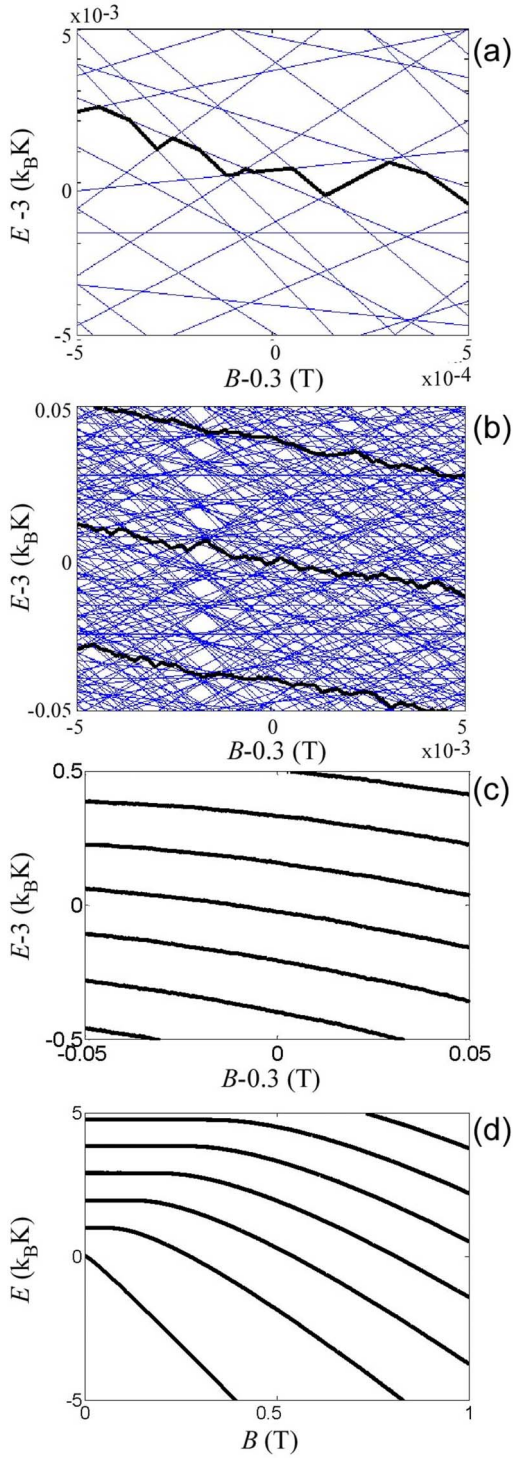

FIG. 5. (Color online) The calculated Zeeman diagram of cluster Co_{12} (assuming $S=12$) with $J_z=0$ in different energy scale. The bold lines are examples of the coupled (adiabatic) levels. The thin lines are the uncoupled levels. (a) The Zeeman diagram in a range $|B-0.3\ \mathrm{T}|\leq 5\times 10^{-4}$ T and $|E/k_B-3\ \mathrm{K}|\leq 5\times 10^{-3}$ K. (b) The Zeeman diagram in a range $|B-0.3\ \mathrm{T}|\leq 5\times 10^{-3}$ T and $|E/k_B-3\ \mathrm{K}|\leq 5\times 10^{-2}$ K. (c) The Zeeman diagram in a range $|B-0.3\ \mathrm{T}|\leq 0.05$ T and $|E/k_B-3\ \mathrm{K}|\leq 0.5$ K. (d) The Zeeman diagram in a range $0\leq B\leq 1$ T and $-5\ \mathrm{K}\leq E/k_B\leq 5$ K. The Zeeman diagrams for larger clusters are similar but with more states. Note that the Zeeman diagrams are not temperature dependent.

2. Low-field limit

For low fields the density of states in Eq. (7) can be expanded;

$$\rho(E^{\mathrm{EVR}})=\rho(E+g\mu_B S_z B)\approx \rho(E)+g\mu_B S_z B\frac{\partial\rho(E)}{\partial E}.$$

Therefore, the magnetization of a single cluster is approximately

$$M_{\mathrm{single}}=\frac{2}{3}\frac{g(\mu_B S)^2 B}{\rho(E)}\frac{\partial\rho(E)}{\partial E}, \tag{9}$$

which is as expected, a function of E and B.

D. Distribution of magnetization of the cluster beam

In the experiments, we accumulate data for many clusters so that in fact we measure the magnetization distribution of the entire cluster beam. As shown in Eq. (7), the magnetization of a single cluster is in general a function of the energy of the cluster and the magnetic field. Assuming that the clusters are in equilibrium with the source at temperature T, the energies of the clusters in the beam follow the Boltzmann distribution,

$$P'(E)=\rho(E^0)\exp(-E^0/k_BT). \tag{10}$$

Here E^0 and E are the energies of the same adiabatic state at zero magnetic field and finite magnetic field B. (The reason we use notation E^0 instead of E^{EVR} here is that for an adiabatic state, especially in the vicinity of the crossing, rotational and magnetic energies are fully mixed. In other words, the adiabatic states are not in general the eigenstates of H_R and $g\mu_B\boldsymbol{SB}$. Therefore, there is no well defined E^{EVR} for a particular adiabatic state. In contrast, the zero-field energy E^0 is always well defined.) In other words, E^0 and E are on different part of the same curve in Fig. 5(d). Note that it is E^0 (energy of the cluster before it enters the magnetic field) instead of E (the energy of the cluster in the magnetic field) that enters the exponent because the population of the clusters is decided when they are created out of the magnetic field and it does not change when clusters traverse the Zeeman diagram. It is important to point out here that the relation between E and E^0 is not trivial because it is the shape of the adiabatic energy state, which cannot be written as an analytical function for the entire range. The distribution of the magnetization can be found by changing the variable of Eq. (10);

$$P(M_{\mathrm{single}})=\left|\frac{\rho(E^0)\exp(-E^0/k_BT)}{\partial M_{\mathrm{single}}/\partial E}\right|. \tag{11}$$

However, this is not really the analytical solution of $P(M_{\mathrm{single}})$ because the relation between E and E^0 is not an analytical function.

1. High-field limit

At high-field limit, according to Eq. (8), M_{single} saturate at a single value $\mu=g\mu_B S$ without any dependence on energy E. Therefore, the denominator in Eq. (11) approaches zero,

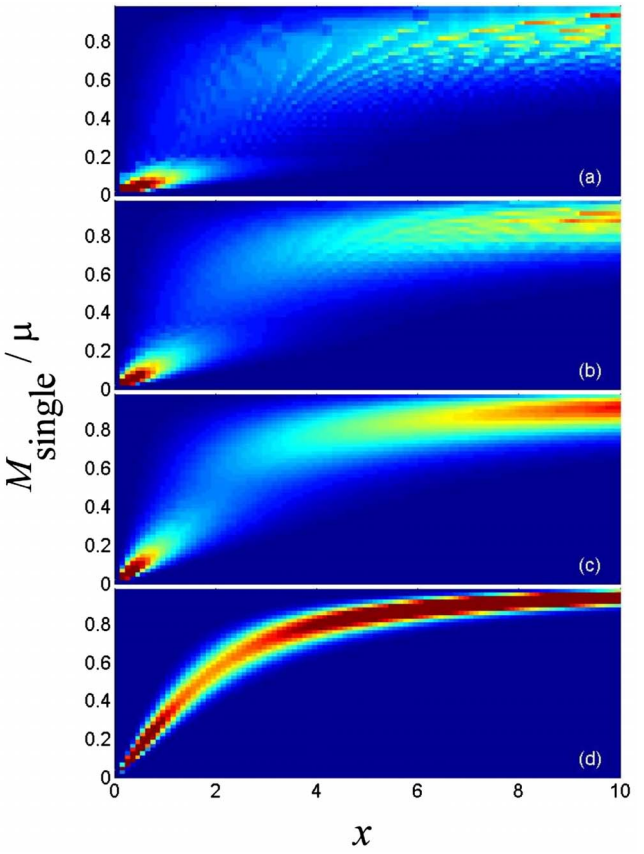

FIG. 6. (Color online) Calculated magnetization distribution for cluster Co_{12} for various conditions as a function of x. (a) $\gamma=0:5$; (b) $\gamma=1$; (c) $\gamma=2$; and (d) $\gamma=20$.

resulting a delta function for the magnetization distribution;

$$P(M_{\text{single}}) = \delta(M_{\text{single}} - \mu). \tag{12}$$

2. Low-field limit

At low-field limit, E^0 may be replaced by E in Eq. (11) to the first-order approximation. The distribution can be found in specific cases analytically. For example, assume $\rho(E) \propto E^{\gamma}$, from Eq. (9) one has

$$M_{\text{single}} = \frac{2}{3}\frac{g(\mu_B S)^2 B}{\rho(E)}\frac{\partial \rho(E)}{\partial E} = \frac{2\gamma}{3}\frac{g(\mu_B S)^2 B}{E}.$$

Hence,

$$P(M_{\text{single}}) \propto \left(\frac{2gS^2\mu_B^2 B\gamma}{3}\right)^{\gamma+1}\frac{1}{M_{\text{single}}^{\gamma+2}}\exp\left(-\frac{2gS^2\mu_B^2 B\gamma}{3k_B T M_{\text{single}}}\right). \tag{13}$$

Note that γ is related to the number of degrees of freedoms that are excited. If no vibrational modes are excited, then $\gamma=0$ (because of the J_z conservation). If one vibrational mode is excited, $\gamma=1$ and so forth. Figure 6 shows the magnetization distribution profile calculated for Co_{12} (assuming $S=12$) under various conditions. The overall behavior of the calculation matches the observed magnetization distribution shown in Fig. 1. One can also see that the distributions depend heavily on γ; the larger the γ, the narrower the distribution.

Note that for high temperature, many vibrational and electronic models are excited, which means that γ is a large number. In this case, the avoided-crossing model predicts a narrow distribution, which is the same as that predicted by the SRM. This plus the fact that avoided-crossing model already predicts the similar average magnetization of the cluster beam suggests that the SRM is the high-temperature limit of the avoided-crossing model.

E. Average of magnetization distribution

As a matter of fact, what has been discussed most by experimental and theoretical works is the average of the magnetization distribution of the cluster beam. Here in the avoided-crossing model, we shall average M_{single} over the ensemble of the cluster beam to compare with experiment. Therefore, by definition the average magnetization of the cluster beam is

$$M = \frac{\int M_{\text{single}} P(M_{\text{single}}) dM_{\text{single}}}{\int P(M_{\text{single}}) dM_{\text{single}}}.$$

It is actually also possible to integrate over the energy distribution using Eq. (10);

$$M = \frac{\int M_{\text{single}} \exp(-E^0/k_B T)\rho(E^0)dE^0}{\int \exp(-E^0/k_B T)\rho(E^0)dE^0}. \tag{14}$$

We shall use Eq. (14) to discuss the high-field and low-field limits.

1. High-field limit

As shown by Eq. (12), the magnetization distribution at high-field limits is a delta function, therefore the average magnetization is

$$M = M_{\text{single}} = g\mu_B S = \mu, \tag{15}$$

which is actually the magnetic moment of the clusters.

2. Low-field limit

In the low-field limit, E^0 may be replaced by E in Eq. (14). Plug Eq. (9) into Eq. (14) for low-field case, the average magnetization of the beam is

$$M = \frac{\int \frac{2gS^2\mu_B^2 B}{3\rho(E)}\frac{\partial \rho(E)}{\partial E}\exp(-E/k_B T)\rho(E)dE}{\int \exp(-E/k_B T)\rho(E)dE}$$

$$= \frac{2gS^2\mu_B^2 B}{3}\frac{\int \frac{\partial \rho(E)}{\partial E}\exp(-E/k_B T)\rho(E)dE}{\int \exp(-E/k_B T)\rho(E)dE}. \tag{16}$$

Integrate Eq. (16) by part, one has

$$M = \frac{4S^2\mu_B^2 B}{3k_B T} = \frac{\mu^2 B}{3k_B T}. \tag{17}$$

Note that this Eq. (17) correspond to the low-field limit of Langevin function [Eq. (1)]. At this point, we can see that both the avoided-crossing model and the SRM predict the Langevin function [Eq. (1)], which matches the experiments very well. Below we show that avoided-crossing model also explains the width of the magnetization distribution quantitatively.

F. Width of the magnetization distribution

Width of the magnetization is defined as $\Delta M = \sqrt{\int (M_{\text{single}} - M)^2 P(M_{\text{single}}) dM_{\text{single}} / \int P(M_{\text{single}}) dM_{\text{single}}}$. In principle, it can be found once the distribution $P(M_{\text{single}})$ is known.

1. High-field limit

As shown by Eq. (12), the magnetization distribution at high-field limits is a delta function. Then it is obvious that the width of magnetization distribution at high-field limit,

$$\Delta M = 0. \tag{18}$$

2. Low-field limit

At low-field limit, we can make use of the magnetization distribution Eq. (13) and the average magnetization Eq. (17). It is not so difficult to find the following:

$$\Delta M = \sqrt{\frac{\int \left(M_{\text{single}} - \frac{\mu^2 B}{3k_B T}\right)^2 P(M_{\text{single}}) dM_{\text{single}}}{\int P(M_{\text{single}}) dM_{\text{single}}}} = \frac{\mu^2 B}{3k_B T}\sqrt{\frac{1}{\gamma - 1}}. \tag{19}$$

Clearly, ΔM approaches zero at low field. Note that Eq. (19) is only for the case that $\gamma > 1$. Equation (19) confirms the observation in Fig. 6; the larger γ, the narrower distribution. In other words, high-temperature beam has a narrow magnetization distribution.

G. Comparison with experiments

We have shown above that the magnetization distribution can be derived analytically at low-field and high-field limits. The results are in good agreement with the experiments. For the intermediate-field range, distribution of magnetization of the cluster beams can be found numerically and compared with experiment.

Figure 6 shows the distribution of magnetization of an ensemble of cluster Co_{12} in a beam as a function of x for low-field, intermediate-field, and high-field conditions assuming a certain γ. Overall, the calculated distributions agree with the experimental observation (see Fig. 1) very well: narrow at low field, broader at intermediate field, and narrow again at high field. The width of the distribution depends on the parameter γ, in other words, the number of degrees of freedom excited in the clusters.

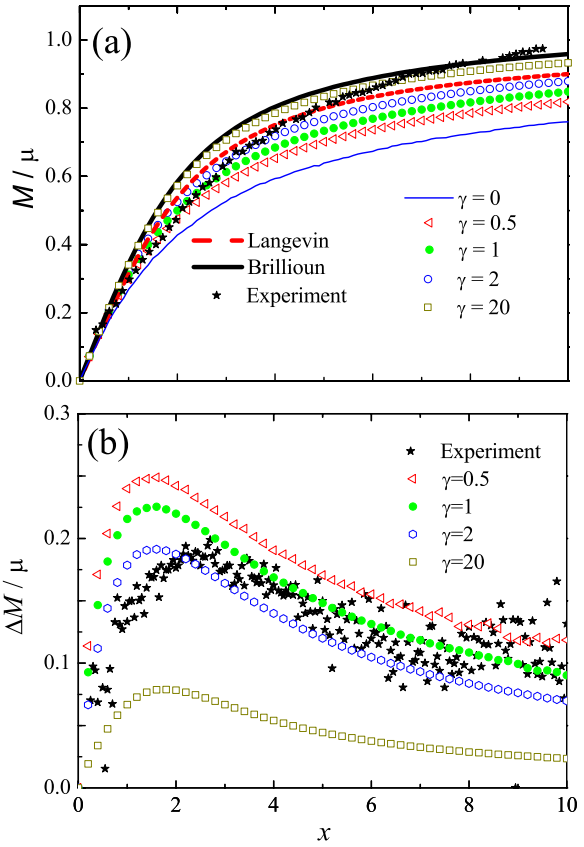

FIG. 7. (Color online) Normalized (a) average and (b) width of magnetization distribution in the beam calculated as a function of x for various γ compared to experimental results.

Figure 7(a) shows the calculated average magnetization as a function of x compared with experiment. Figure 7(b) shows the calculated and the experimental values of ΔM. Note that the width of magnetization distribution is narrower for larger γ. From the comparison between experiment and calculation, there should be only a couple of phonons excited in the measured clusters, which confirms that there are not enough vibrational and electronic modes excited to form a heat bath in our experiment.

V. DISCUSSION

We should emphasize again that the avoided-crossing model is to provide more comprehensive understandings of the magnetization behavior of ferromagnetic cluster beams. Actually, the avoided-crossing model and the SRM predict the similar behavior of average magnetization, and for low-temperature beam, the avoided-crossing model agrees with experiment much better. However, at high-temperature limit, the two models predict very similar results that are consistent with the experiment, which is an indication that the SRM is the high-temperature limit of the avoided-crossing model. In fact, it is not so difficult to understand the similarity of the

two models at high temperature. At high temperature, the most populated states are in the high-energy part of the Zeeman diagram. Clusters in those states have lots of excited vibrational and electronic degrees of freedoms. Therefore, for very R_z and S_z combination, there are so many interacting states that the energy separations between the states are very small. Because of the small energy separations, Landau-Zener tunnelings (see Appendix C) occur frequently when clusters traverse the Zeeman diagram, which is similar to the thermalization between different degrees of freedom of the clusters. In addition to that, in the high-energy part of the Zeeman diagram, the energy states are mostly parallel, which is the reason that the distribution of the magnetization is narrow. Furthermore, when lots of degrees of freedom are excited, temperature may be defined for an isolated cluster, which is close to the ensemble temperature. However still, an isolated cluster itself should be considered as a microcanonical ensemble, in which total energy is more essential and always well defined. Using the language of nonlinear physics, the system becomes more irregular and the ergodicity increases when more degrees of freedoms are activated. When the system is ergodic, simple thermodynamics works.[33]

Our previous paper[18] about the average magnetization of cobalt cluster beams and the avoided-crossing model has attracted attention. Recently, Payne *et al.*[34] also revisited the cobalt cluster beams and entered the discussion of the mechanism of the magnetization. We hereby clarify a few confusing issues that may cause misunderstandings.

It is the broad magnetization of small clusters in low-temperature beams that motivated us to pursuit a more comprehensive picture of the magnetization of cluster beam. Indeed, the result we have (the avoided-crossing model) is not an alternative model but a more general model, which works much better than the SRM for small clusters in a low-temperature beam and converges to the SRM at high-temperature limit. In other words, the avoided-crossing model also works when there are lots of vibrational and electronic degrees of freedoms excited, as shown in the above discussion.

It is undisputable that the quantum confinement causes the discreteness of the vibrational and the electronic spectra, producing the spectra cutoff (gap) at low energy.[35] It is also true that clusters have lower melting temperatures than the bulk, suggesting lower Debye temperatures.[36,37] However, these differences will not eliminate the cutoff. In fact, far-infrared spectra of small niobium clusters show clear cutoffs, and the vibrational modes are all very close to the $k_B T_{\mathrm{Debye}}$.[38] After all, for an ensemble temperature 20 K, a 2-meV gap is enough to quench the clusters to the ground state. Even if a couple of modes happen to have low energy (which is not likely the case for metal clusters), they cannot act like heat bath for low-energy clusters.

The spin-rotation coupling is discussed in the avoided-crossing model because it is the most relevant one. Clusters start from the source with random spin orientations and end up with biased spin orientations after negotiating with the magnetic field. In order to change orientation of the spins and conserved the total angular momentum, clusters have to get the angular momentum needed from their rotations because there is no other possibilities. This requires that the spin and rotation degrees of freedoms have to be coupled by, namely, spin-rotation coupling. There can be many other coupling in the clusters (see Appendices A and B), e.g., spin-body axis coupling (from magnetocrystalline anisotropy). However, everything has to come down to the effective spin-rotation coupling to contribute to the spin reorientation. Small spin-rotation coupling is assumed in Sec. IV, which is justified in Appendix A. However, it is also shown that the conclusion actually holds even when the coupling is not much weaker than the Zeeman energy and the rotational energy separation because the repulsion between the states keeps the topology of the Zeeman diagram very similar to the low coupling case. In other words, as long as the avoided crossings hold, the Zeeman diagram is similar and all of the above conclusions are the same.

We insist that the relevant temperature in the Lagevin function [Eq. (1)] is the ensemble temperature. Every individual clusters does not necessarily have well defined temperature. This is especially true for isolated low-energy small clusters whose energy separations are large. High-energy large clusters have smaller energy separations and more excited degrees of freedom. In this case, temperature may be defined and is very close to the ensemble temperature. Rotational temperature is by no means the only temperature considered in the avoided-crossing model. Temperature does not affect the Zeeman diagram, it only plays a role when the Zeeman diagram is populated according to Eq. (10), where the E^0 is a linear combination of rotational, vibrational, and electronic energies. Suppose there are some cooling effects on rotations making the rotational temperature smaller, the exponent in Eq. (10) becomes $\exp(-E_R/T_R - E_{EV}/T)$, where E_R, T_R, and E_{EV} are the rotational energy, rotational temperature, and electronic and vibrational energies, including all the activated modes. Only when T/T_R is comparable to E_{EV}/E_R, the difference between T_R and T has an impact on the magnetization. Considering the angular momentum conservation, for a specific J_z, there are only two rotational modes. In other words, the rotation cooling does not affect the magnetization, unless all the electronic and vibrational excitations are quenched or almost quenched. These extreme conditions are achieved for small clusters in low-temperature beams. We have a good reason to believe that the cooling effect on the rotational temperature is minimal in our cluster beams that are quasieffusive with a large velocity slip.[39] In fact, the good agreement between the theoretical calculation and the experiments confirms that.

VI. CONCLUSION

We have studied the distribution of magnetization of cobalt cluster beams over a wide range of cluster sizes ($12 \leq N \leq 200$), temperatures ($20 \leq T \leq 100$ K), and magnetic fields ($0 \leq B \leq 2$ T). We also proposed an avoided-crossing model, which turns out to be able to explain the magnetization distribution quantitatively. Therefore, the spin-relaxation paradox is resolved. In summary, the single-sided deflections of cobalt clusters are in general due to the repulsions between the adiabatic states that reduce the magnetization. The

broadening of the detected beam profiles is caused by the magnetization distributions. It is also shown that the SRM is a high-temperature limit of the avoided-crossing theory.

ACKNOWLEDGMENTS

We gratefully acknowledge financial support from the National Science Foundation.

APPENDIX A: COUPLING STRENGTH IN COBALT CLUSTERS

We should be concerned with the coupling term H_{couple} in Hamiltonian of Eq. (5). First, we should emphasize that the details of the coupling is complicated especially for asymmetric clusters. Here we only discuss the orders of magnitude of the coupling strength for some special cases.

Ignoring the nuclear spin, the general form of the coupling is

$$H_{\text{couple}} = \alpha_{SR}\mathbf{S}\cdot\mathbf{R} + \alpha_{SA}(\mathbf{S}\cdot\mathbf{A})^2,$$

where $\mathbf{R}$ is the rotation of the cluster, $\mathbf{A}$ is one of the body axes of the cluster (assuming single axis anisotropy), and α_{SR} and α_{SA} are the strength for spin-rotation coupling and for the spin-body axis coupling, respectively. For weak coupling the approximate eigenstates are $|R,R_z,R_a,S,S_z\rangle$, where R_z and R_a are the projection of $\mathbf{R}$ on the magnetic field and the body axis $\mathbf{A}$, respectively. The off-diagonal terms are

$$\langle R',R'_z,R'_a,S',S'_z|H_{\text{couple}}|R,R_z,R_a,S,S_z\rangle \propto \delta_{S_z+R_z,S'_z+R'_z},$$

which cause avoided crossings of the unperturbed states.

The electron spin couples to its orbital motion intrinsically (spin-orbit coupling). For an atom in a cluster or in the bulk, the crystal field is not spherically symmetric. The reduced symmetry of the crystal field gives the orbital motion of the electrons a preferred direction. The magnetic anisotropy energy depends on the spin-orbit coupling strength and the crystal fields.[40] If the spin-orbit coupling strength is larger than the crystal-field energy, then the orbital angular momentum is still a good quantum number. This is the case for rare-earth metal. The crystal field will cause spin-body axis coupling, which is reflected in the anisotropy energy. If the effect of crystal field is larger than the effect of spin-orbit coupling, then the orbital angular momentum will be quenched. In this case the anisotropy energies are small. This is the case for iron group metals.

For a cluster in a beam, we also have to take into account the mass rotations.[41,42] Rotational angular momentum tends to uncouple the electronic spin angular momentum from the body axis and for large rotations, and the spin couples to the rotations. There are two important mechanisms for the spin-rotation coupling.[41] In one, the rotation of the cluster generates a magnetic field parallel to the axis of rotation. Classically, the coupling energy can be treated as the energy of a magnetic dipole moment in a magnetic field, thus,

$$\Delta_{SR} \approx \frac{N\mu_B\mu_0 e\omega}{r},$$

where μ_0 is the vacuum magnetic permeability, ω is the angular frequency of the cluster rotation, and r is the radius of the cluster. The average angular frequency of the cluster depends on the rotational temperature as $\frac{2}{5}mr^2\omega^2 = 3k_BT$. For our experimental conditions, the coupling energy is on the order of 10^{-7} eV and it is larger for smaller clusters and higher temperatures.

Spin-orbit coupling also causes an indirect coupling of the electronic spin to the rotation. According to van Vleck,[42] the energy of this second-order process is

$$\Delta_{SR} \sim \frac{C_r\Delta_{SO}}{\Delta_e},$$

where C_r is the rotation constant, Δ_{SO} is the spin-orbit coupling strength, and Δ_e is the energy needed to excite the electrons to higher angular momentum states. If the Δ_e is from the collective rotation of the electrons in the cluster, $C_r/\Delta_e \sim 10^{-3}$. The spin-orbit coupling energy for an electron is about 10^{-4} eV; therefore we get $\Delta_{SR} \sim 10^{-7}$ eV.

Recall from Eq. (5) that $|H_{\text{mag}}| \approx gS_z\mu_B$ is on the order of μB. For our experiments, $\mu \approx 2\mu_B N$ and $B \sim 1$ T. Hence, $H_{\text{mag}} \sim 10^{-3}$ eV is much larger than the spin-rotation coupling strength. Thus, the approximation we made earlier is justified; the coupling can be treated as a perturbation.

APPENDIX B: STRONG-COUPLING CASES

For iron group metal clusters, we can treat the couplings as perturbations. Still there are other cases in which the coupling energy is stronger than the Zeeman energy H_{mag}. One example is the clusters with strong spin axis coupling or large anisotropy energy. Some rare-earth metal clusters fall into this category. The other case is from clusters with large spin-rotation coupling, which occurs for very small clusters because they rotate very fast.[41]

For the case of strong spin-body axis coupling, we can consider the electronic spin fixed to one of the body axes. The Hamiltonian will be similar to Eq. (5),

$$H = H_E + H_V + H_R + H_{\text{couple}} - g\mu_B SB\frac{J_zJ_a}{J(J+1)},$$

where J is the total angular momentum including electronic spin and cluster rotations; J_z and J_a are the projection of $\mathbf{J}$ on magnetic field and body axis, respectively.[41] We can follow the same procedure as we did for Eq. (5). Again in the Zeeman diagram, we will see many level crossings. The spin-rotation coupling H_{couple} at the degenerate point for the levels with same J_z will cause the crossing to be avoided. Therefore, if clusters follow these levels adiabatically, we should see a very similar behavior as in the weak-coupling case. Hamamoto *et al.*[30] have shown that this is indeed the case. The low-field average magnetization is also similar to that described by Eq. (1). However, Hamamoto *et al.* ignored that the magnetization is measured within a finite range of magnetic fields; so they concluded the magnetization distribution should be wide and clusters should show negative deflections. In fact, the experimental averaging mechanism causes narrow widths. For example, magnetic deflection experiments on holmium clusters that have large anisotropy energy do not show negative magnetic deflections at all.[43]

For strong spin-rotation coupling case, we can consider the electronic spin to be perfectly aligned with the cluster rotation; in other words $J=S+R$, therefore,

$$H = H_E + H_V + H_R + H_{\text{couple}} - g\mu_B SB\frac{J_z}{J},$$

which means that the magnetization distribution is uniform, spanning from $-\mu$ to μ.[41] Again, when the level crossings are avoided, the magnetization distribution will change significantly. Although the quantitative magnetization distribution in this case has not yet been studied in detail, one would expect the similar Zeeman diagram as long the crossings are avoided. In other words, all the conclusions from the avoided crossing models should hold.

APPENDIX C: LANDAU-ZENER TUNNELING

We have assumed that the clusters traverse their energy states adiabatically. In fact, if the magnetic field changes with a finite speed dB/dt, there is a probability to make Landau-Zener transition between E_i^{couple} and E_j^{couple}.[44] For the case in Fig. 4 the transition rate is given by

$$P_{LZ} = \exp\left(-\frac{2\pi\Delta_{SR}^2}{\mu_B h|S_z - S_z'|dB/dt}\right) = \exp\left(-\frac{\Delta_{SR}^2}{\Delta_{LZ}^2}\right),$$

$$\text{where} \quad \Delta_{LZ} = \sqrt{\frac{\mu_B h|S_z - S_z'|dB/dt}{2\pi}}.$$

For typical experiments, we find $dB/dt \approx 50$ T/s, therefore $\Delta_{LZ} \sim 10^{-8}$ eV. Then Δ_{SR} is greater than Δ_{LZ}, hence $p_{LZ} \sim 0$, which means that the Landau-Zener transitions are not important. In other words, the process is at least approximately adiabatic.

Actually, the process does not have to be totally adiabatic for the conclusion to hold. We can estimate the number of crossings within the measurement range,

$$n_{\text{crossing}} \approx \frac{\mu\Delta B}{C_r},$$

where ΔB is the field change in the measurement range. For a typical experiment, we find for cluster Co_{100} that $N_{\text{crossing}} \approx 1000$. Even if only one of these crossings is actually avoided, the average magnetization will still show significant reduction compared to totally uncoupled cases.

[1] D. M. Cox, D. J. Trevor, R. L. Whetten, E. A. Rohlfing, and A. Kaldor, Phys. Rev. B **32**, 7290 (1985).
[2] W. A. de Heer, P. Milani, and A. Chatelain, Phys. Rev. Lett. **65**, 488 (1990).
[3] J. P. Bucher, D. C. Douglass, and L. A. Bloomfield, Phys. Rev. Lett. **66**, 3052 (1991).
[4] D. C. Douglass, A. J. Cox, J. P. Bucher, and L. A. Bloomfield, Phys. Rev. B **47**, 12874 (1993).
[5] A. J. Cox, J. G. Louderback, and L. A. Bloomfield, Phys. Rev. Lett. **71**, 923 (1993).
[6] J. P. Bucher and L. A. Bloomfield, Int. J. Mod. Phys. B **7**, 1079 (1993).
[7] A. J. Cox, J. G. Louderback, S. E. Apsel, and L. A. Bloomfield, Phys. Rev. B **49**, 12295 (1994).
[8] I. M. L. Billas, A. Chatelain, and W. A. Deheer, Science **265**, 1682 (1994).
[9] S. E. Apsel, J. W. Emmert, J. Deng, and L. A. Bloomfield, Phys. Rev. Lett. **76**, 1441 (1996).
[10] T. Hihara, S. Pokrant, and J. A. Becker, Chem. Phys. Lett. **294**, 357 (1998).
[11] M. B. Knickelbein, Phys. Rev. Lett. **86**, 5255 (2001).
[12] S. Pokrant and J. A. Becker, Eur. Phys. J. D **16**, 165 (2001).
[13] S. Pokrant and J. A. Becker, J. Magn. Magn. Mater. **226–230**, 1921 (2001).
[14] M. B. Knickelbein, Phys. Rev. B **70**, 014424 (2004).
[15] R. Moro, S. Yin, X. Xu, and W. A. de Heer, Phys. Rev. Lett. **93**, 086803 (2004).
[16] M. B. Knickelbein, Phys. Rev. B **71**, 184442 (2005).
[17] S. Yin, X. Xu, R. Moro, and W. A. de Heer, Phys. Rev. B **72**, 174410 (2005).
[18] X. Xu, S. Yin, R. Moro, and W. A. de Heer, Phys. Rev. Lett. **95**, 237209 (2005).
[19] M. B. Knickelbein, J. Chem. Phys. **125**, 044308 (2006).
[20] C. P. Bean and J. D. Livingston, J. Appl. Phys. **30**, S120 (1959).
[21] S. N. Khanna and S. Linderoth, Phys. Rev. Lett. **67**, 742 (1991).
[22] J. Merikoski, J. Timonen, M. Manninen, and P. Jena, Phys. Rev. Lett. **66**, 938 (1991).
[23] P. Ballone, P. Milani, and W. A. de Heer, Phys. Rev. B **44**, 10350 (1991).
[24] P. J. Jensen and K. H. Bennemann, Ber. Bunsenges. Phys. Chem. **96**, 1233 (1992).
[25] A. Maiti and L. M. Falicov, Phys. Rev. B **48**, 13596 (1993).
[26] G. F. Bertsch and K. Yabana, Phys. Rev. A **49**, 1930 (1994).
[27] G. Bertsch, N. Onishi, and K. Yabana, Z. Phys. D: At., Mol. Clusters **34**, 213 (1995).
[28] P. J. Jensen and K. H. Bennemann, Z. Phys. D: At., Mol. Clusters **35**, 273 (1995).
[29] V. Visuthikraisee and G. F. Bertsch, Phys. Rev. A **54**, 5104 (1996).
[30] N. Hamamoto, N. Onishi, and G. Bertsch, Phys. Rev. B **61**, 1336 (2000).
[31] M. B. Knickelbein, J. Chem. Phys. **121**, 5281 (2004).

[32] We use the E^0 and E^{uncouple} for the coupled (perturbed) states, E^{EVR} and E^{uncouple} $(=E^{EVR}\text{-}g\mu_B S_z B)$ for the uncoupled states. The symbol E is used for a general energy in the Zeeman diagram. For uncoupled states, electronic, vibrational and rotational degrees of freedom are separable. For such a state, there is well defined E^{EVR}, that is, the electronic, vibrational and rotational energies. It is not the case for the coupled states. Another reason we want to distinguish the two zero field energy is that if one starts from a point with energy E and magnetic field B in the Zeeman diagram and trace down to zero field, he will get E^{EVR} if he follows the uncoupled state, E^0 if he follows the coupled

states. Those two are generally two different points on the *y*-axis.
[33] P. Pechukas, Phys. Rev. Lett. **51**, 943 (1983).
[34] F. W. Payne, W. Jiang, J. W. Emmert, J. Deng, and L. A. Bloomfield, Phys. Rev. B **75**, 094431 (2007).
[35] W. P. Halperin, Rev. Mod. Phys. **58**, 533 (1986).
[36] M. Schmidt, R. Kusche, B. von Issendorff, and H. Haberland, Nature (London) **393**, 238 (1998).
[37] G. A. Breaux, C. M. Neal, B. Cao, and M. F. Jarrold, Phys. Rev. Lett. **94**, 173401 (2005).
[38] A. Fielicke, C. Ratsch, G. von Helden, G. Meijer, J. Chem. Phys. **127**, 234306 (2007).
[39] X. S. Xu, Ph.D. thesis, Georgia Institute of Tecnhology, 2007.
[40] R. C. O'Handley, *Modern Magnetic Materials: Principles and Applications* (Wiley, New York, 2000).
[41] C. H. Townes and A. L. Schawlow, *Microwave Spectroscopy* (Dover, New York, 1975).
[42] J. H. Vanvleck, Rev. Mod. Phys. **23**, 213 (1951).
[43] S. Y. Yin, X. S. Xu, R. Moro, W. A. de Heer (unpublished).
[44] C. Zener, Proc. R. Soc. London, Ser. A **137**, 696 (1932).